

# Mean-field dynamical density functional theory

J Dzubiella and C N Likos<sup>§</sup>

University Chemical Laboratory, Lensfield Road, Cambridge CB2 1EW,  
United Kingdom

**Abstract.** We examine the out-of-equilibrium dynamical evolution of density profiles of ultrasoft particles under time-varying external confining potentials in three spatial dimensions. The theoretical formalism employed is the dynamical density functional theory (DDFT) of Marini Bettolo Marconi and Tarazona [J. Chem. Phys. **110**, 8032 (1999)], supplied by an equilibrium excess free energy functional that is essentially exact. We complement our theoretical analysis by carrying out extensive Brownian Dynamics simulations. We find excellent agreement between theory and simulations for the whole time evolution of density profiles, demonstrating thereby the validity of the DDFT when an accurate equilibrium free energy functional is employed.

Density functional theory (DFT) is a very powerful tool for the quantitative description of the equilibrium states of many-body systems under arbitrary external fields. It rests on the exact statement that the Helmholtz free energy of the system,  $F[\rho]$ , is a unique functional of the inhomogeneous one-particle density  $\rho(\mathbf{r})$ . Moreover, the equilibrium profile  $\rho_0(\mathbf{r})$  minimises  $F[\rho]$  under the constraint of fixed particle number  $N$  [1]. The task is then to approximate the unknown functional  $F[\rho]$  from which all equilibrium properties of the system follow. Much more challenging is the problem of studying *out-of-equilibrium dynamics* of many-body systems, for which analogous uniqueness and minimisation principles are lacking. In this paper, we present results based on a recently-proposed dynamical density functional theory (DDFT) formalism and we demonstrate that the latter is capable of describing out-of-equilibrium diffusive processes in colloidal systems at the Brownian time scale.

We are concerned with the dynamics of typical soft-matter systems, such as suspensions of mesoscopic spheres and polymer chains in a microscopic solvent [2]. The enormous difference in the masses of the suspended particles and the solvent molecules implies a corresponding separation in the relaxational time scales of the two. At times of the order of the Fokker-Planck scale,  $\tau_{\text{FP}} \sim 10^{-14}$  sec, the solvent coordinates are long relaxed to thermal equilibrium. On the Brownian diffusive time scale,  $\tau_{\text{B}} \sim 10^{-9}$  sec, the momentum coordinates of the solute particles relax to equilibrium with the heat bath of the solvent molecules and thus a statistical description involving only the positions of the colloids is feasible [3]. In this regime, the evolution of the coordinates

<sup>§</sup> Also at: Institut für Theoretische Physik II, Heinrich-Heine-Universität Düsseldorf, Universitätsstraße 1, D-40225 Düsseldorf, Germany

$\{\mathbf{r}_1(t), \mathbf{r}_2(t), \dots, \mathbf{r}_N(t)\}$  of the  $N$  colloidal particles is described by the set of stochastic Langevin equations:

$$\frac{d\mathbf{r}_i(t)}{dt} = -\Gamma \nabla_{\mathbf{r}_i} \left[ \sum_{j \neq i} V(|\mathbf{r}_i - \mathbf{r}_j|) + V_{\text{ext}}(\mathbf{r}_i, t) \right] + \mathbf{w}_i(t). \quad (1)$$

In Eq. (1) above,  $V(|\mathbf{r}_i - \mathbf{r}_j|)$  is the pair (effective) interaction potential between the mesoscopic particles [2],  $V_{\text{ext}}(\mathbf{r}_i, t)$  is the externally acting potential and  $\mathbf{w}_i(t) = [w_i^x(t), w_i^y(t), w_i^z(t)]$  is a stochastic term representing the random collisions with the solvent molecules and having the properties:

$$\langle w_i^\alpha(t) \rangle = 0 \quad \text{and} \quad \langle w_i^\alpha(t) w_j^\beta(t') \rangle = 2D \delta_{ij} \delta_{\alpha\beta} \delta(t - t'), \quad (2)$$

where the averages  $\langle \dots \rangle$  are over the Gaussian noise distribution and  $\alpha, \beta = x, y, z$ , the Cartesian components. The constants  $\Gamma$  and  $D$  stand for the mobility and diffusion coefficients of the particles, respectively, and the Einstein relation gives  $\Gamma/D = (k_B T)^{-1} \equiv \beta$ . Applying the rules of the Itô stochastic calculus, Marconi and Tarazona [4, 5] recasted the above equations into the form

$$\Gamma^{-1} \frac{\partial \rho(\mathbf{r}, t)}{\partial t} = \nabla_{\mathbf{r}} \left[ k_B T \nabla_{\mathbf{r}} \rho(\mathbf{r}, t) + \rho(\mathbf{r}, t) \nabla_{\mathbf{r}} V_{\text{ext}}(\mathbf{r}, t) \right] + \nabla_{\mathbf{r}} \left[ \int d^3 r' \langle \hat{\rho}(\mathbf{r}, t) \hat{\rho}(\mathbf{r}', t) \rangle \nabla_{\mathbf{r}} V(\mathbf{r} - \mathbf{r}') \right]. \quad (3)$$

Here,  $\hat{\rho}(\mathbf{r}, t) = \sum_i \delta(\mathbf{r}_i(t) - \mathbf{r})$  is the usual one-particle density operator and  $\rho(\mathbf{r}, t) = \langle \hat{\rho}(\mathbf{r}, t) \rangle$  is the noise-average of this quantity. Up to this point, all is exact. Now, the following *physical assumption* (A) is introduced: as the system follows its relaxative dynamics, the instantaneous two-particle correlations can be approximated with those of a system in thermodynamic equilibrium with the same, *static* one-particle density  $\rho(\mathbf{r})$  as the noise-averaged dynamical one-particle density  $\rho(\mathbf{r}, t)$ . Then, Eq. (3) can be cast into a form involving exclusively the *equilibrium* density functional  $F[\rho]$  as [4, 5]

$$\Gamma^{-1} \frac{\partial \rho(\mathbf{r}, t)}{\partial t} = \nabla_{\mathbf{r}} \cdot \left[ \rho(\mathbf{r}, t) \nabla_{\mathbf{r}} \frac{\delta F[\rho(\mathbf{r}, t)]}{\delta \rho(\mathbf{r}, t)} \right], \quad (4)$$

with the free energy functional

$$F[\rho] = k_B T \int d^3 r \rho(\mathbf{r}) \{ \ln [\rho(\mathbf{r}) \Lambda^3] - 1 \} + F_{\text{ex}}[\rho] + \int d^3 r V_{\text{ext}}(\mathbf{r}, t) \rho(\mathbf{r}). \quad (5)$$

The dynamical equation of motion (4) was in fact first derived in a phenomenological way by Dieterich, Frisch and Majhofer [6].

In carrying out concrete calculations with the theory put forward above and in comparing them with Brownian Dynamics (BD) simulation results based on the microscopic equations of motion, Eq. (1), two sources of possible discrepancies exist: first, the fundamental assumption (A) and second the approximate nature of the equilibrium density functional  $F_{\text{ex}}[\rho]$  of Eq. (5). In this work we focus our attention to *ultrasoft particles* for which a very accurate and simple functional  $F[\rho]$  is known, namely the *mean-field* or *random-phase approximation* (RPA) functional given by Eq. (6) below.

This guarantees that one can explore the accuracy of the fundamental assumption (A) under well-defined external conditions.

Consider a one-component system of ultrasoft particles. It has been demonstrated that for such systems the following RPA-functional is quasi-exact [7, 8, 9, 10, 11, 12, 13]:

$$F_{\text{ex}}[\rho] = \frac{1}{2} \int \int d^3r d^3r' V(|\mathbf{r} - \mathbf{r}'|) \rho(\mathbf{r}) \rho(\mathbf{r}'). \quad (6)$$

Eq. (4) takes now with the help of Eqs. (5) and (6) the form

$$\begin{aligned} \Gamma^{-1} \frac{\partial \rho(\mathbf{r}, t)}{\partial t} = & k_B T \nabla_{\mathbf{r}}^2 \rho(\mathbf{r}, t) + \nabla_{\mathbf{r}} \rho(\mathbf{r}, t) \cdot \int d^3r' \nabla_{\mathbf{r}} V(|\mathbf{r} - \mathbf{r}'|) \rho(\mathbf{r}', t) \\ & + \rho(\mathbf{r}, t) \int d^3r' \nabla_{\mathbf{r}}^2 V(|\mathbf{r} - \mathbf{r}'|) \rho(\mathbf{r}', t) \\ & + \nabla_{\mathbf{r}} \rho(\mathbf{r}, t) \cdot \nabla_{\mathbf{r}} V_{\text{ext}}(\mathbf{r}, t) + \rho(\mathbf{r}, t) \nabla_{\mathbf{r}}^2 V_{\text{ext}}(\mathbf{r}, t). \end{aligned} \quad (7)$$

Given an initial density field  $\rho(\mathbf{r}, t = 0)$  and a prescribed external potential  $V_{\text{ext}}(\mathbf{r}, t)$ , Eq. (7) can be numerically solved to yield  $\rho(\mathbf{r}, t)$ . In this work we apply an ultrasoft Gaussian pair potential between the interacting particles that has been shown to describe the effective interaction between the centres of mass of polymer chains in athermal solvents [9, 14]

$$V(r) = \epsilon \exp[-(r/\sigma)^2]. \quad (8)$$

We set  $\epsilon = k_B T$  providing the energy unit for the problem, whereas  $\sigma$ , which corresponds to the gyration radius of the polymers, will be the unit of length henceforth. Accordingly, the natural time scale of the problem, providing the unit of time in this work, is the Brownian time scale  $\tau_B = \sigma^2/(\epsilon\Gamma)$ . Eq. (7) is solved using standard numerical techniques, and for a variety of time-dependent confining external potentials  $V_{\text{ext}}(\mathbf{r}, t)$  to be specified below.

Brownian Dynamics simulations of Eq. (1) are also straightforward to carry out. The Langevin equations of motion including the external field are numerically solved using a finite time-step  $\Delta t = 0.003 \tau_B$  in all simulations, and the technique of Ermak [15, 16]. In order to obtain the time-dependent density  $\rho(\mathbf{r}, t)$  we perform a large number  $N_{\text{run}}$  of independent runs, typically  $N_{\text{run}} = 5000$ , and average the density profile over all configurations for a fixed time  $t$ .

We focus to external fields that correspond to a sudden change, i.e.,  $V_{\text{ext}}(\mathbf{r}, t) = \Phi_1(\mathbf{r})\Theta(-t) + \Phi_2(\mathbf{r})\Theta(t)$ . These force the system to relax from the equilibrium density  $\rho_1(\mathbf{r}) = \rho(\mathbf{r}, t < 0)$ , compatible to the external potential  $\Phi_1(\mathbf{r})$ , to the new equilibrium density  $\rho_2(\mathbf{r}) = \rho(\mathbf{r}, t \rightarrow \infty)$ , corresponding to the external potential  $\Phi_2(\mathbf{r})$ . Important questions related to such processes are what is the typical relaxation time  $\tau$  for such a procedure and how does the system cross over from one equilibrium density to the other. We consider two kinds of confinements: spherical ones,  $V_{\text{ext}}(\mathbf{r}, t) = V_{\text{ext}}(r, t)$ , where  $r = |\mathbf{r}|$ , and planar ones between two walls perpendicular to the  $z$ -Cartesian direction,  $V_{\text{ext}}(\mathbf{r}, t) = V_{\text{ext}}(z, t)$ . In these cases we obtain  $\rho(\mathbf{r}, t) = \rho(r, t)$  and  $\rho(\mathbf{r}, t) = \rho(z, t)$ , correspondingly, and the solution of Eq. (7) is greatly simplified since the integrals take

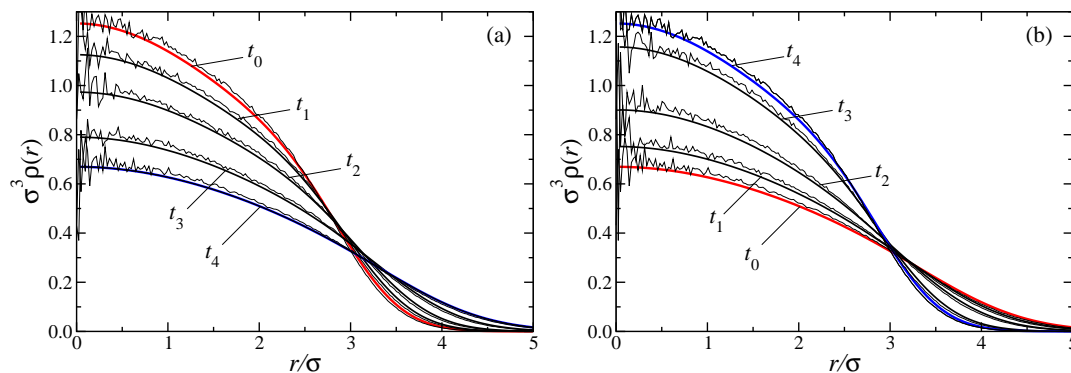


**Figure 1.** DDFT (solid lines) and BD (noisy lines) results for the time development of the radial density profiles  $\rho(r)$  in the spherical confining potential  $V_{\text{ext}}^{(1)}(r, t)$  with (a)  $R_1 = 4.0$  and  $R_2 = 6.0$  and (b)  $R_1 = 6.0$  and  $R_2 = 4.0$ . The shown profiles are for the times  $t_0 = 0$ ,  $t_1 = 0.06$ ,  $t_2 = 0.18$ ,  $t_3 = 0.54$  and  $t_4 = 2.0$ , all in  $\tau_B$ -units. The last time is practically equivalent to  $t = \infty$ , since the system there has fully relaxed into equilibrium. In all figures, red curves denote the initial and blue ones the final static profile.

the form of one-dimensional convolutions that can be evaluated very rapidly by use of fast Fourier transform techniques.

Three different external confinements have been specifically investigated. Two spherical ones

$$V_{\text{ext}}^{(1)}(r, t) = \Phi_0 [(r/R_1)^2 \Theta(-t) + (r/R_2)^2 \Theta(t)]; \quad (9)$$

$$V_{\text{ext}}^{(2)}(r, t) = \Phi_0 [(r/R_1)^{10} \Theta(-t) + (r/R_2)^{10} \Theta(t)]; \quad (10)$$

and one slab confinement

$$V_{\text{ext}}^{(3)}(z, t) = \Phi_0 [(z/Z_1)^{10} \Theta(-t) + \phi(z/Z_2)^{10} \Theta(t)]. \quad (11)$$

The energy scale  $\Phi_0$  sets the strength of the confining potential and is fixed to  $\Phi_0 = 10 k_B T$  for all three confinements. The only difference between the external potential for times  $t < 0$  and for  $t > 0$  lies in the different length scales  $R_2 \neq R_1$  for Eqs. (9) and (10), and  $Z_1 \neq Z_2$  for Eq. (11). For each confinement we consider two cases that give rise to two different dynamical processes:  $R_1 < R_2$  ( $Z_1 < Z_2$ ), enforcing an *expansion* of the system and  $R_1 > R_2$  ( $Z_1 > Z_2$ ), bringing about a *compression* of the same. For the spherical confinements an additional parameter is the particle number  $N = \int d^3r \rho(r, t)$  which is a conserved quantity, as is clear from Eq. (4) that has the form of a continuity equation.  $N$  enters the formalism through the normalisation of the density field at  $t = 0$ . For both spherical confinements the particle number is  $N = 100$ . In the slab confinement, Eq. (11), the conserved quantity is the density per unit area  $\rho_0 = \int dz \rho(z, t)$ . We choose  $\rho_0 \sigma^2 = 10$ . In all cases examined, the typical relaxation time was found to be of order  $\tau_B$ ; after typically  $t = 2 \tau_B$ , the system fully relaxes into the new equilibrium profile.

In Fig. 1 we show the results for the harmonic confining potential of Eq. (9). It can be seen that the theory reproduces the time evolution of the density profile, both for the

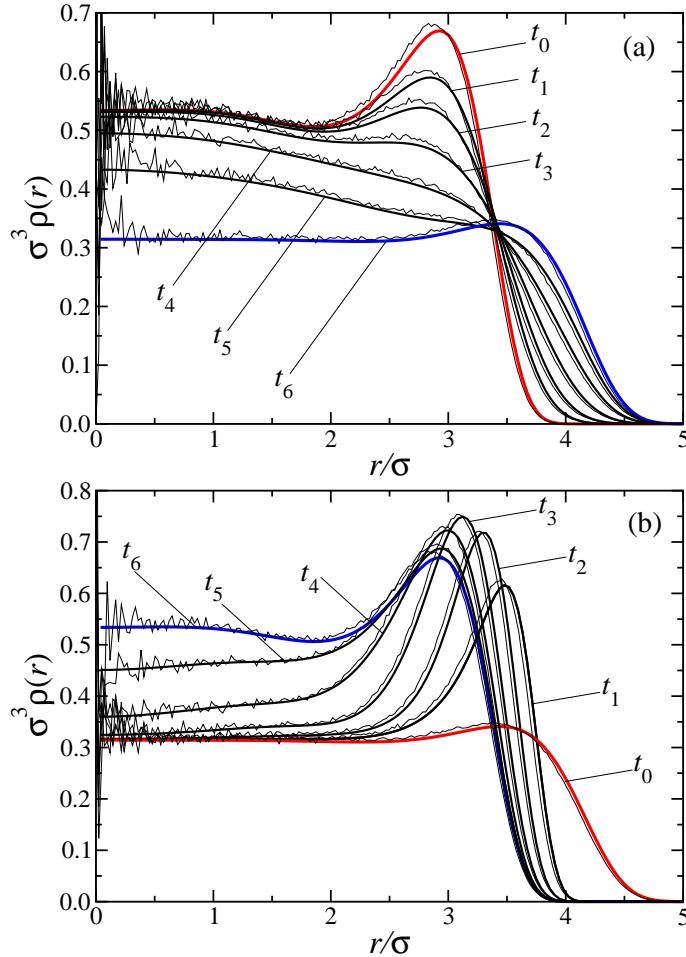


**Figure 2.** DDFT (solid lines) and BD (noisy lines) results for the time development of the radial density profiles  $\rho(r)$  in the spherical confining potential  $V_{\text{ext}}^{(2)}(r, t)$  with (a)  $R_1 = 4.0$  and  $R_2 = 5.0$  and (b)  $R_1 = 5.0$  and  $R_2 = 4.0$ . The shown profiles are for the times  $t_0 = 0$ ,  $t_1 = 0.03$ ,  $t_2 = 0.06$ ,  $t_3 = 0.12$ ,  $t_4 = 0.24$ ,  $t_5 = 0.48$  and  $t_6 = 2.0$  (in units of  $\tau_B$ ).

expansion [Fig. 1(a)] and the compression [Fig. 1(b)] processes. An asymmetry in the two processes can be already discerned: the compression is not the ‘time reversed’ of the expansion and this effect will be much stronger in the examples to follow. Though the profiles of the system are considerably different from those of an ideal gas, i.e., effects of the interparticle interaction are present, the confining potential is smooth enough, so that the profiles are devoid of pronounced correlation peaks.

The situation is different for the external potential of Eq. (10). Here, the power-law dependence is much more steep, so that the Gaussian fluid develops correlation peaks close to the ‘walls’ of the confining field. The dynamical development of the profiles for the expansion and compression processes are shown in Fig. 2. Here, the asymmetry between the expansion and the compression processes is evident. In the former case, seen in Fig. 2(a), the expansion of the confining potential leaves behind

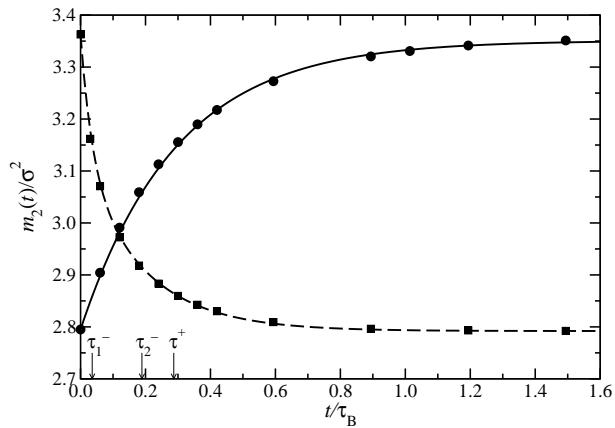


**Figure 3.** The second moment of the radial density profile,  $m_2(t)$ , defined in Eq. (12) plotted against the time  $t$  for the spherical confinement  $V_{\text{ext}}^{(2)}(r, t)$ . Circles correspond to radii  $R_1 = 4.0$  and  $R_2 = 5.0$  (expansion) and squares show the resulting curve for the inverse process,  $R_1 = 5.0$  and  $R_2 = 4.0$  (compression). The lines are the analytical fits shown in the text. Solid line: Eq. (13); long-dashed line: Eq. (14). The arrows mark the characteristic time scales defined in these two equations.

a density profile that has very strong density gradients close to the boundary of the initial confinement. Since the latter ceases to act at  $t = 0$ , this leaves at  $t = 0^+$  instantaneously a region  $R_1 < r < R_2$  that is devoid of particles but in which the new external potential is essentially zero. This leads to a collective diffusion of the particles towards the boundaries set by the new potential. Correspondingly, the high density peaks decrease rapidly and leak outward. In the inner region,  $r \approx 0$  of the profile, the dynamics is much slower and the relaxation to the final plateau there takes place at the end of the process, causing thereby the final development of the new, weaker correlation peaks close to the location of the boundary,  $r \lesssim R_2$ .

The compression process, depicted in Fig. 2(b) runs very differently. There, the initial ‘closing’ of the potential from  $R_1$  to  $R_2 < R_1$  leaves at  $t = 0^+$  a region of high density at  $R_1 < r < R_2$  that now finds itself within a strongly repulsive external field. There is an extremely rapid shrinking there, accompanied by the development of very high correlation peaks that actually ‘overshoot’ in height with respect to the final equilibrium profile. Initially, the region in the centre of the sphere remains unaffected and only as the high peaks start diffusing does material flow toward the centre and at the latest stage of the dynamics the profile at  $r = 0$  reaches its new equilibrium value.

In order to quantify better this asymmetry and also extract characteristic time scales for the two dynamical processes, we consider the second moment of the density,  $m_2(t)$ , defined through

$$m_2(t) = \int d^3r r^2 \rho(r, t). \quad (12)$$

The quantity  $m_2(t)$  is a quantitative measure of the spread of  $\rho(r, t)$  around the centre of the external field and its time evolution is shown in Fig. 3. Let the superscript

‘+’ denote the expansion and the superscript ‘-’ the compression process. Obviously, it holds  $m_2^\pm(0) = m_2^\mp(\infty)$ . We notice that for both processes  $m_2(t)$  is a monotonic function of  $t$  but some interesting differences arise when one fits the two curves by analytic functions, shown as lines in Fig. 3. The expansion can be very accurately described by a single exponential:

$$m_2^+(t) = m_2^+(0) + [m_2^+(\infty) - m_2^+(0)][1 - \exp(-t/\tau^+)], \quad (13)$$

with the characteristic time scale  $\tau^+ = 0.287 \tau_B$ . However, a double-exponential fit is necessary to parameterise the compression process, namely

$$m_2^-(t) = m_2^-(\infty) + A^- \exp(-t/\tau_1^-) + [m_2^-(0) - m_2^-(\infty) - A^-] \exp(-t/\tau_2^-), \quad (14)$$

with the fit parameter  $A^- = 0.240 \sigma^{-2}$  and the *two* characteristic time scales  $\tau_1^- = 0.036 \tau_B$  and  $\tau_2^- = 0.189 \tau_B$ . Since  $\tau_{1,2}^- < \tau^+$ , it follows that the compression process is at any rate faster than the expansion one. The occurrence of the two distinct time scales  $\tau_1^- \ll \tau_2^-$  in the compression requires some explanation. The fast process that takes place at times  $t \sim \tau_1^-$  corresponds to the abrupt shrinking of the profile at the wings of the distribution and is caused exclusively by the ‘closing’ of the external field. This is the same mechanism that brings about the overshooting of the density peaks. Once this is over, diffusion within the now already confined system takes place and the second characteristic time scale,  $\tau_2^-$ , is solely determined by the interaction potential  $V(r)$  and the average particle density. In the expansion process, the first mechanism is absent thus a single time scale,  $\tau^+$ , shows up, which is of intrinsic origin exclusively. Since stronger density gradients occur during the compression than during the expansion process, even the larger of the two time scales of the compression,  $\tau_2^-$ , is smaller than  $\tau^+$ . The denser the system is, the faster the collective diffusion towards equilibrium.

Finally, we turn our attention to the slab confinement. The results from theory and simulation are shown in Fig. 4. Once more it can be seen that the DDFT offers an excellent description of the dynamics of the system. The same asymmetry between expansion and compression that was seen in the spherical confinement also shows up for the case of the slab, including the overshooting of the peaks during the compression process. In addition, the density profiles develop during their evolution secondary oscillations that are also very well reproduced by the theory.

In summarising, we have demonstrated that the dynamical density functional theory of Marini Bettolo Marconi and Tarazona [4, 5], when supplemented by an accurate equilibrium density functional, can provide an excellent description of out-of-equilibrium dynamics of colloidal systems at the Brownian time scale. The accuracy of the DDFT formalism has already been successfully tested for the system of one-dimensional hard rods [4], for which the exact density functional  $F[\rho]$  is known. To the best of our knowledge, this is the first study of the validity of DDFT in three dimensions. As the phenomenology in 3d is much richer than in 1d, including the possibility of phase transitions, many intersecting ways for future applications open up.

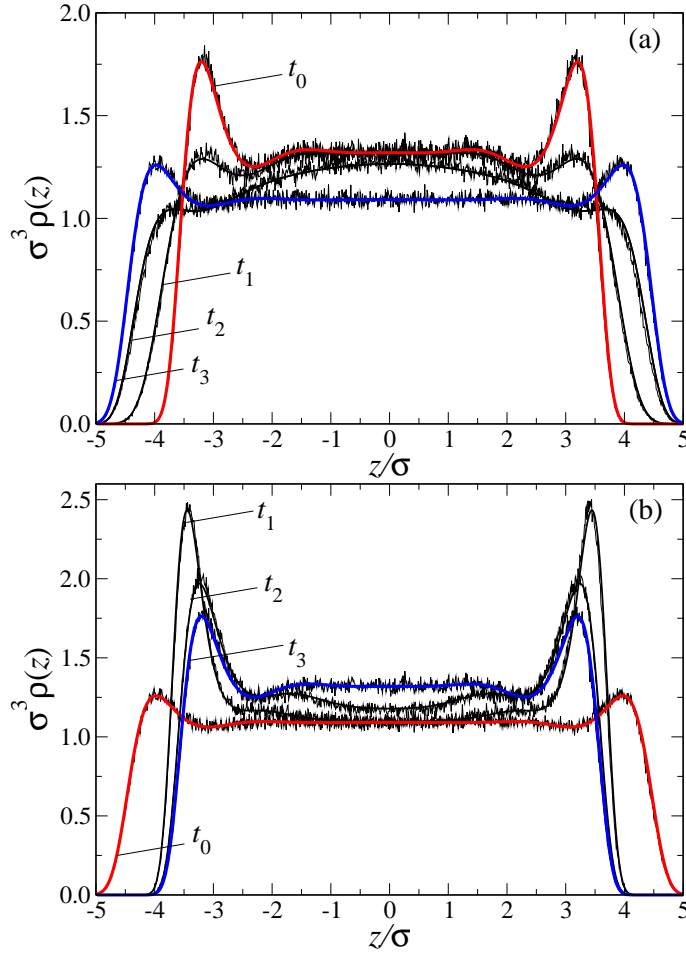


**Figure 4.** DDFT (solid lines) and BD (noisy lines) results for the time development of the linear density profile  $\rho(z)$  in a slab confining potential  $V_{\text{ext}}^{(3)}(z, t)$  with (a)  $Z_1 = 4.0$  and  $Z_2 = 5.0$  and (b)  $Z_1 = 5.0$  and  $Z_2 = 4.0$ . The shown profiles are for the times  $t_0 = 0, t_1 = 0.06, t_2 = 0.24$  and  $t_3 = 2.0$  (in units of  $\tau_B$ ).

## Acknowledgments

Discussions with Andrew Archer, Bob Evans, Wolfgang Dieterich and Pedro Tarazona are gratefully acknowledged. This work has been supported by the Deutsche Forschungsgemeinschaft through the SFB TR6.

## References

- [1] Evans R 1979 *Adv. Phys.* **28** 143
- [2] Likos C N 2001 *Phys. Rep.* **348** 267
- [3] Dhont J K G 1996 *An Introduction to Dynamics of Colloids* (Amsterdam:Elsevier)
- [4] Marini Bettolo Marconi U and Tarazona P 1999 *J. Chem. Phys.* **110** 8032
- [5] Marini Bettolo Marconi U and Tarazona P 2000 *J. Phys.: Condens. Matter* **12** A413
- [6] Dieterich W, Frisch H L and Majhofer A 1990 *Z. Phys. B* **78** 317
- [7] Lang A, Likos C N, Watzlawek M and Löwen H 2000 *J. Phys.: Condens. Matter* **12** 5087

- [8] Likos C N, Lang A, Watzlawek M and Löwen H 2001 *Phys. Rev. E* **63** 031206
- [9] Louis A A, Bolhuis P G and Hansen J P 2000 *Phys. Rev. E* **62** 7961
- [10] Archer A J and Evans R 2001 *Phys. Rev. E* **64** 041501
- [11] Archer A J and Evans R 2002 *J. Phys.: Condens. Matter* **14** 1131
- [12] Archer A J, Likos C N and Evans R 2002 *J. Phys.: Condens. Matter* **14** 12031
- [13] Archer A J, Evans R and Roth R 2002 *Europhys. Lett.* **59** 526
- [14] Louis A A, Bolhuis P G, Hansen J P and Meijer E J 2000 *Phys. Rev. Lett.* **85** 2522
- [15] Allen M P and Tildesley T J 1989 *Computer Simulation of Liquids* (Clarendon Press: Oxford)
- [16] Ermak D L 1975 *J. Chem. Phys.* **62** 4189